Chemical Physics 119 (1988) 159–170
North-Holland, Amsterdam

TRANSLATIONAL SPECTROSCOPY OF THE TRIATOMIC DICATIONS CO_2^{2+}, OCS^{2+} AND CS_2^{2+}

P. JONATHAN, M. HAMDAN, A.G. BRENTON

Mass Spectrometry Research Unit, University College of Swansea, Singleton Park, Swansea SA2 8PP, UK

and

G.D. WILLETT

School of Chemistry, University of New South Wales, P.O.Box 1, Kensington, NSW 2033, Australia

Received 5 August 1987

Measurement of single-electron capture (SEC) and translational energy spectroscopy (TES) of the triatomic dications CO_2^{2+}, OCS^{2+}, CS_2^{2+} at high product ion resolution (typically 0.6 eV) is facilitated by a novel translational spectrometer. Calibration of SEC spectra allows the detection and precise assignment of observed state-selective processes; TES data indicate the presence of dication states having the same spin symmetry. Since single and double ionisation of each triatomic neutral ACB (where A and B represent O and S) to low-lying cation states occurs by removal of essentially non-bonding electrons, the bond lengths and energies of each of ACB, ACB^+ and ACB^{2+} are similar. Therefore, current data permit the evaluation of electronic levels of the triatomic dications in excellent agreement with previous experimental and theoretical work. A systematic procedure for future investigations of multiply charged molecular ions is proposed.

1. Introduction

The triatomic dications CO_2^{2+}, OCS^{2+} and CS_2^{2+} have received considerable experimental attention, culminating in the recent publication by Millie et al. [1], in which the current experimental data concerning these species are summarised; information from Auger [2], double-charge transfer (DCT) [1] and photoion–photoion coincidence [1], together with electron impact [3–8] and photoionisation [9,10] mass spectroscopy is cited. Moreover, since these triatomic dications ACB^{2+} (where A and B represent O and S, abbreviation (A, B) = (O, S)) are of sufficient simplicity, they are accessible to ab initio SCF CI calculations, also reported by Millie et al. [1]. In the present article, we report investigations of CO_2^{2+}, OCS^{2+} and CS_2^{2+}, involving keV single-electron capture (SEC) and collisional excitation/translational energy spectroscopy (TES), using a novel translational spectrometer [11,12], providing further energetic data.

1.1. Single-electron capture (SEC)

Studies of state-selective keV single-charge transfer between atomic species have been extended recently to include molecular targets [13] and projectiles [14–18]. For dicationic projectiles, capture cross section maximises for reaction pathways with moderate exothermicities of ≈ 1.5 to ≈ 5.0 eV, corresponding to SEC via avoided crossings of adiabatic potential energy surfaces. We examine reactions of the form

$$A\vec{C}B^{2+} + R \rightarrow A\vec{C}B^{+} + R^{+} \qquad (1)$$

where (A, B) = (O, S) and R is a rare-gas atom. The $\rightarrow$ superscript denotes a fast (keV) ion. For an exothermic process, the product ions gain

0301-0104/88/$03.50

tional energy ΔE due to the release of internal excitation energy

$$\Delta E = E_v(ACB^{2+} \rightarrow ACB^{+}) - E_v(R \rightarrow R^{+}), \quad (2)$$

where $E_v(Y \rightarrow Z)$ represents the absolute energy change associated with the vertical transition $Y \rightarrow Z$. Here, $E_v(R \rightarrow R^+)$ is the ionisation energy of R, and $E_v(ACB^{2+} \rightarrow ACB^+)$ is the vertical recombination energy of ACB^{2+}. In practice, the translational energy gain of R^+ is negligibly small [19], so that ΔE represents the translational energy gain of ACB^+. By selecting the target species R so that $\Delta E \approx 1.5$–5.0 eV for transitions involving the ground (and any excited) projectile states, those transitions will be manifested as peaks in the resulting ACB^+ translational energy distributions. Precise calibration of the translational energy scale, facilitated by use of an internal standard (see section 3), permits accurate measurements (± 0.2 eV) of ΔE values, so that the recombination energy $E_v(ACB^{2+} \rightarrow ACB^+)$ is obtainable to the same precision. Recalling the relation

$$E_v(ACB^{2+} \rightarrow ACB^{+}) = E_{el}(ACB^{2+}) + E_{vib}(ACB^{2+}) - [E_{el}(ACB^{+}) + E_{vib}(ACB^{+})], \quad (3)$$

where E_{el} and E_{vib} are the respective electronic and vibrational energies of the molecular ion states involved, we deduce that the double-ionisation energy of ACB takes the form

$$E_{el}(ACB^{2+}) = E_v(ACB^{2+} \rightarrow ACB^{+}) + E_{el}(ACB^{+}) - [E_{vib}(ACB^{2+}) - E_{vib}(ACB^{+})]. \quad (4)$$

Provided, therefore, that the difference in reactant and product vibrational energies is small, and that the final molecular state ACB^+ is known, then the double-ionisation energy $E_{el}(ACB^{2+})$ can be deduced. Other evaluations [16,17] of double-ionization energies for diatomic dications based on the above principle have given excellent agreement with existing data.

Further, the relative shifts of peaks in the ACB^+ translational energy distribution are independent of the energy scale calibration (and the precision to which this calibration is performed), so that the difference in the exothermicities of various single-electron capture processes can be measured with even higher accuracy (± 0.05 eV) in most cases. Consequently, the excitation energies of electronically excited ACB^{2+} states can be determined. By reducing the ionising electron energy E_e (in the ion source) then the metastable fractions in the projectile beam are also reduced, so that SEC processes involving the ground and excited states of ACB^{2+} can be distinguished.

1.2. Collisional excitation / translational energy spectroscopy (TES)

The technique of collisional excitation spectroscopy, or translational energy spectroscopy (TES) provides collision-induced transition energies to high precision [20], facilitating the deduction of excitation energies for atomic [20–22] and molecular [23–25] species. Grazing collisions between a keV beam of ACB^{2+} and a target (usually He) induce observable vertical transitions between the quantised energy levels of the projectile (or possibly the target; for a He target, however, this is extremely unlikely). These transitions cause discrete detectable changes $\Delta' E$ in the projectile translational energy; both superelastic and inelastic processes can be observed in this way. For a transition from state Y to state Z of ACB^{2+}

$$\vec{ACB}^{2+}(Y) + He \rightarrow \vec{ACB}^{2+}(Z) + He, \quad (5)$$

then

$$\Delta' E = E_v(ACB^{2+}(Y) \rightarrow ACB^{2+}(Z)) \quad (6a)$$

$$= E_{el}(ACB^{2+}(Y)) - E_{el}(ACB^{2+}(Z)) + [E_{vib}(ACB^{2+}(Y)) - E_{vib}(ACB^{2+}(Z))]. \quad (6b)$$

TES transitions, the most probable of which occur at $|\Delta' E| < 5$ eV, have been shown (e.g. ref. [24]) to weakly obey the electric dipole selection rules; spin-conserving transitions tend to dominate, although spin-changing transitions are observed [26] especially when spin–orbit coupling becomes significant; the orbital angular momentum quantum number change accompanying a transition is not

restricted to 0, ± 1 (so that $\Sigma \rightarrow \Delta$ processes are observed, for example ref. [24]). In the present investigation, TES is used in conjunction with SEC to ascertain excitation energies for CO_2^{2+}, OCS^{2+} and CS_2^{2+}.

2. Experimental

Experiments were performed on a novel double-focusing translational spectrometer [11] based on a symmetrical arrangement of two identical cylindrical electrostatic analysers. The instrument and its performance have been described elsewhere [12]; however a schematic diagram is given in fig. 1 to help understand its mode of operation in these experiments.

ACB^{2+} dications are formed by $E_e = 100$ eV electron impact of the appropriate precursor (CO_2, OCS and CS_2), maintained at a source pressure of ≈ 0.1 Pa and at a source temperature of 450 K. They are extracted and accelerated through 3 kV (i.e. to a translational energy of 6 keV). The dication ACB^{2+} is mass selected by the magnetic sector (MAG) and allowed to pass into the "double-focusing" energy analysis stage (ESA1 and ESA2), the ion optical properties of which are such as to given excellent first- and second-order energy and angular focusing properties [11,27]. A gas collision cell (CC in fig. 1), within which target gas is maintained at an estimated pressure of 10^{-3} Pa, is located between the two electric sectors. Fast molecular products of collision reactions (1) or (5) between the projectile ACB^{2+} ions and the target gas are detected using an electron multiplier (D2, see fig. 1) by scanning the post-collision analysers ESA2 and ESA3 in tandem over the appropriate voltage range ($\approx 2U$ for SEC and $\approx U$ for TES, where U is the high voltage applied to the ion source, $U = 3$ kV here). The small energy analyser (ESA3, see fig. 1) is used to eliminate various low level interferences caused by ion fragmentation within ESA2 and ion (or neutral) reflections off the walls of ESA2 or the resolving slit S3 reaching the detector [28].

The present apparatus is capable of excellent translational energy resolution, compared with similar keV sector-based designs. For example [12],

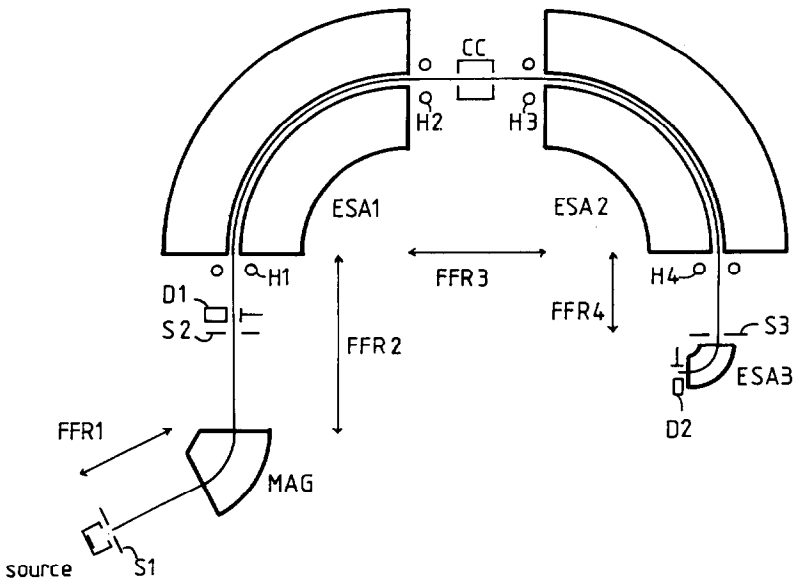

Fig. 1. Schematic diagram of the translational energy spectrometer: S1, S2 and S3 – focal plane resolving slits; D1 and D2 – electron multiplier detectors; FFR – field free region; H1–H4 – electric hexapole lenses; CC – collision cell; MAG – magnetic sector; ESA – electrostatic analyser.

spin–orbit splitting of Ar^+ (0.18 eV) has been resolved by 6 keV Ar^{2+}–He SEC, and TES routinely permits the detection of spin–orbit transitions (0.67 eV) in Kr^+. For the present molecular ion systems, translational energy differences of 0.6 eV are comfortably separated by SEC and TES.

3. Results

3.1. SEC

As proposed in section 1, the charge-transfer target species R (see (1)) was preselected so that state-selective processes of interest would appear with substantial cross sections in the resulting translational energy distributions for molecular products ACB^+; for example, previous electron impact studies (see table 1) suggest a double-ionisation energy of ≈ 38 eV for CO_2, so we expect (see (3)) that the recombination energy $E_v(CO_2^{2+}(\tilde{X}) \rightarrow CO_2^+(\tilde{X}))$ is ≈ 24 eV. (Here we have used the standard abbreviated spectroscopic notation $\tilde{X}$ for the ground electronic state.) Therefore, by selecting Ne as target gas, with first ionisation energy of 21.6 eV, the exothermicity for ground state–ground state capture, given by (2), is ≈ 2 eV, ensuring a reasonable cross section for this specific capture channel. By extending this argument, it was decided to study the CO_2^{2+}–Ne, OCS^{2+}–Ar and CS_2^{2+}–Ar SEC collision systems, in order to:

(i) measure the double-ionisation energies of CO_2, OCS and CS_2 respectively; and

(ii) measure the excitation energies of CO_2^{2+}, OCS^{2+} and CS_2^{2+} respectively.

The crucial experiment facilitating the first measurement above, namely the evaluation of $E_{el}(ACB^{2+})$, is that of translational energy scale calibration. It was found that consistent, accurate calibration is possible by means of internal standard measurements, such as the 6 keV Ar^{2+}–Ne and Kr^{2+}–Ar SEC systems, the spectra for which are well known (refs. [31,32] respectively). This choice of calibrant projectiles is particularly convenient since the mass-to-charge ratios of Ar^{2+} (20) and $^{84}Kr^{2+}$ (42) neatly encompass those of CO_2^{2+} (22), OCS^{2+} (30) and CS_2^{2+} (38). Therefore, good agreement between the two calibration systems would reasonably imply that the calibration was also applicable to the triatomic dication systems. A small amount of Ar (or Kr) gas was added to the source sample, and the spectra for capture by ACB^{2+} and Ar^{2+} (or Kr^{2+}) were recorded consecutively by adjusting the magnet current. In the present investigation, the calibration offset, arising from contact potentials and other

Table 1
Appearance energies (eV) for triatomic dications

Ion	Photon impact	Electron impact	Double-charge transfer [a]	Charge stripping [b]	Charge transfer [c]
$CO_2^{2+}(\tilde{X}\,^3\Sigma_g^-)$	36.7 [d]	37.6 [e]	37.7(±0.2)	38.3	37.4(±0.3)
$OCS^{2+}(\tilde{X}\,^3\Sigma^-)$	–	30.0 [f]	30.7(±0.2)	28.0	29.8(±0.4)
$CS_2^{2+}(\tilde{X}\,^3\Sigma_g^-)$	27.3 [g]	25.5 [h]	27.4(±0.1)	28.1	27.5(±).3

[a] Ref. [1]. DCT gives $E_v(ACB(\tilde{X}\,^1\Sigma^+) \rightarrow ACB^{2+}(\tilde{a}\,^1\Delta))$. This value is reduced by $E_v(ACB^{2+}(\tilde{a}\,^1\Delta) \rightarrow ACB^{2+}(\tilde{X}\,^3\Sigma^-))$ to yield the energy given here.

[b] Ref. [29]. Charge stripping gives $|E_v(ACB^+(\tilde{X}\,^2\Pi) \rightarrow ACB^{2+}(\tilde{X}\,^3\Sigma^-))|$. This value is increased by the first ionisation energy of ACB to yield the energy given here.

[c] Present work. Charge transfer (SEC) gives the recombination energy $E_v(ACB^{2+}(\tilde{X}\,^3\Sigma^-) \rightarrow ACB^+(\tilde{X}\,^2\Pi))$, which must be increased by the first ionisation energy of ACB to yield the energy given here.

[d] Ref. [1]. Average of three values. Standard deviation (SD) = 0.68.

[e] Ref. [1]. Average of seven values. SD = 0.72.

[f] Ref. [6].

[g] Ref. [1]. Average of two values. SD = 0.05.

[h] Ref. [30].

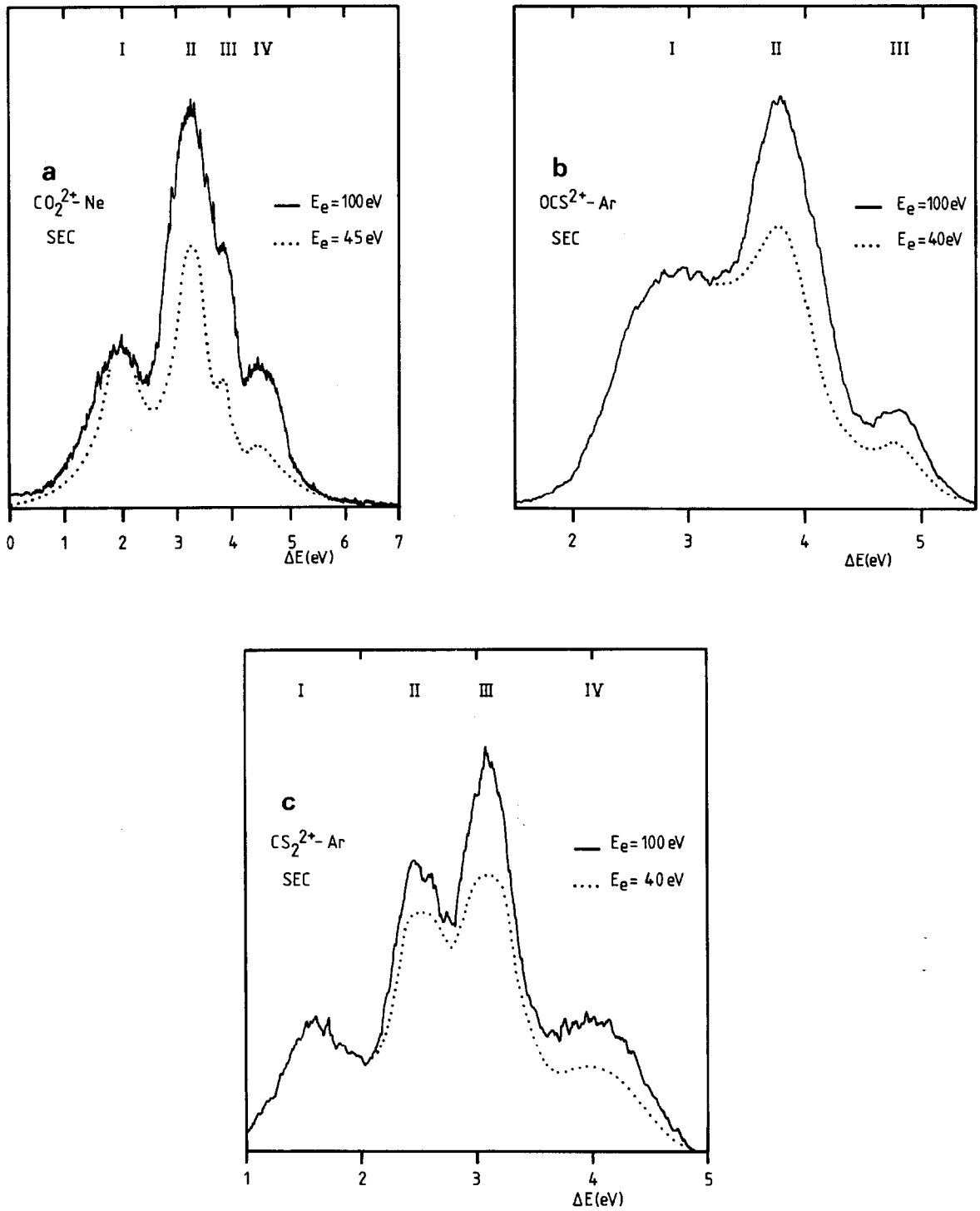

Fig. 2. Translational energy for 6 keV SEC collisions between: (a) CO_2^{2+} and Ne at $E_e = 100$ eV (and 45 eV), (b) OCS^{2+} and Ar at $E_e = 100$ eV (and 40 eV), (c) CS_2^{2+} and Ar at $E_e = 100$ eV (and 40 eV).

Table 2
Summary of SEC data

Capture system	Exothermicities ΔE (eV) of observed channels				Energy differences (eV) between channels		
	O–I [a]	O–II	O–III	O–IV	I–II	II–III	III–IV
CO_2^{2+}–Ne	2.0(±0.3)	3.3(±0.3)	3.9(±0.4)	4.7(±0.3)	1.3(±0.2)	0.6(±0.3) [b]	0.8(±0.3)
OCS^{2+}–Ar	2.8(±0.4) [c]	3.8(±0.3)	4.8(±0.3)	–	1.0(±0.3)	1.0(±0.1)	–
CS_2^{2+}–Ar	1.6(±0.3)	2.5(±0.3)	3.1(±0.3)	4.1(±0.3)	0.9(±0.1)	0.6(±0.1)	1.9(±0.2)

[a] O denotes the position, on the calibrated translational energy scale, of a resonant SEC process.
[b] Peak II is difficult to precisely locate; $|II-IV| = 1.4(\pm 0.2)$ eV.
[c] Unusually broad peak, signifying substantial vibrational population.
[d] Peaks are particularly narrow; vibrational structure visible in some spectra.

effects was -1.2 ± 0.2 eV, applicable to all SEC spectra; the remaining indeterminancy in ascribing the exact exothermicity of a given capture process is the peak width (see fig. 2). Vibrational excitation generally introduces an uncertainty of at least about ± 0.05 eV in the exact location of peak centres, due to the broadening of SEC spectra; this problem becomes particularly acute when two capture channels lie within ≈ 0.3 eV to one another (e.g. peaks II and III of fig. 2a). The resulting increased imprecision of our measurements is reflected in the values in table 2, which gives a summary of the data assimilated from the spectra in fig. 2.

The current experimental spectra exhibit a number of peaks, labelled by the Roman numericals I, II, III (and IV if necessary) in fig. 2, probably involving capture not only from $ACB^{2+}(\tilde{X})$, but also from electronically excited states such as $ACB^{2+}(\tilde{A})$, $ACB^{2+}(\tilde{a})$, ... Conclusive identification of processes involving ground-state projectiles was obtained by reducing the source ionising electron energy E_e from its normal operating value of 100 eV down to near the threshold energy for formation of ACB^{2+}; SEC spectra recorded at low E_e are outlined by dots in fig. 2. Results indicate that peak I increases in intensity, with respect to all others, as the value of E_e is lowered, suggesting that process I in each case is due to capture from $ACB^{2+}(\tilde{X})$. In greater detail, fig. 3 shows the percentage intensities of peaks, II, III (and IV) relative to peak I, normalised to their intensities in the dotted spectra of fig. 2, as a function of E_e near the appearance

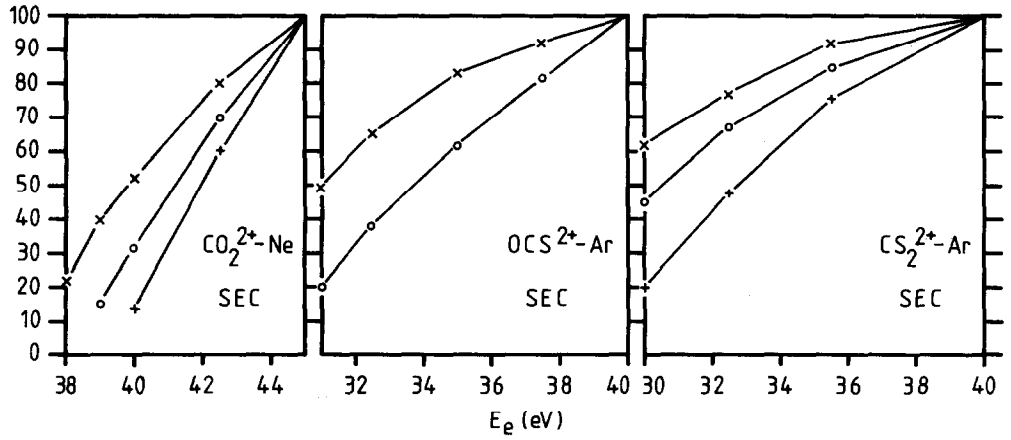

Fig. 3. Percentage intensities of peaks II (×), III (○) and IV (+) relative to peak I, normalised to their intensities at $E_e = 45$ eV (for CO_2^{2+}–Ne SEC) and $E_e = 40$ eV (for OCS^{2+}–Ar SEC and $CS_2^{2+} \rightarrow$ Ar SEC). (Peak I, if shown, would contribute a straight line parallel to the absicca axis at a percentage relative intensity of 100.)

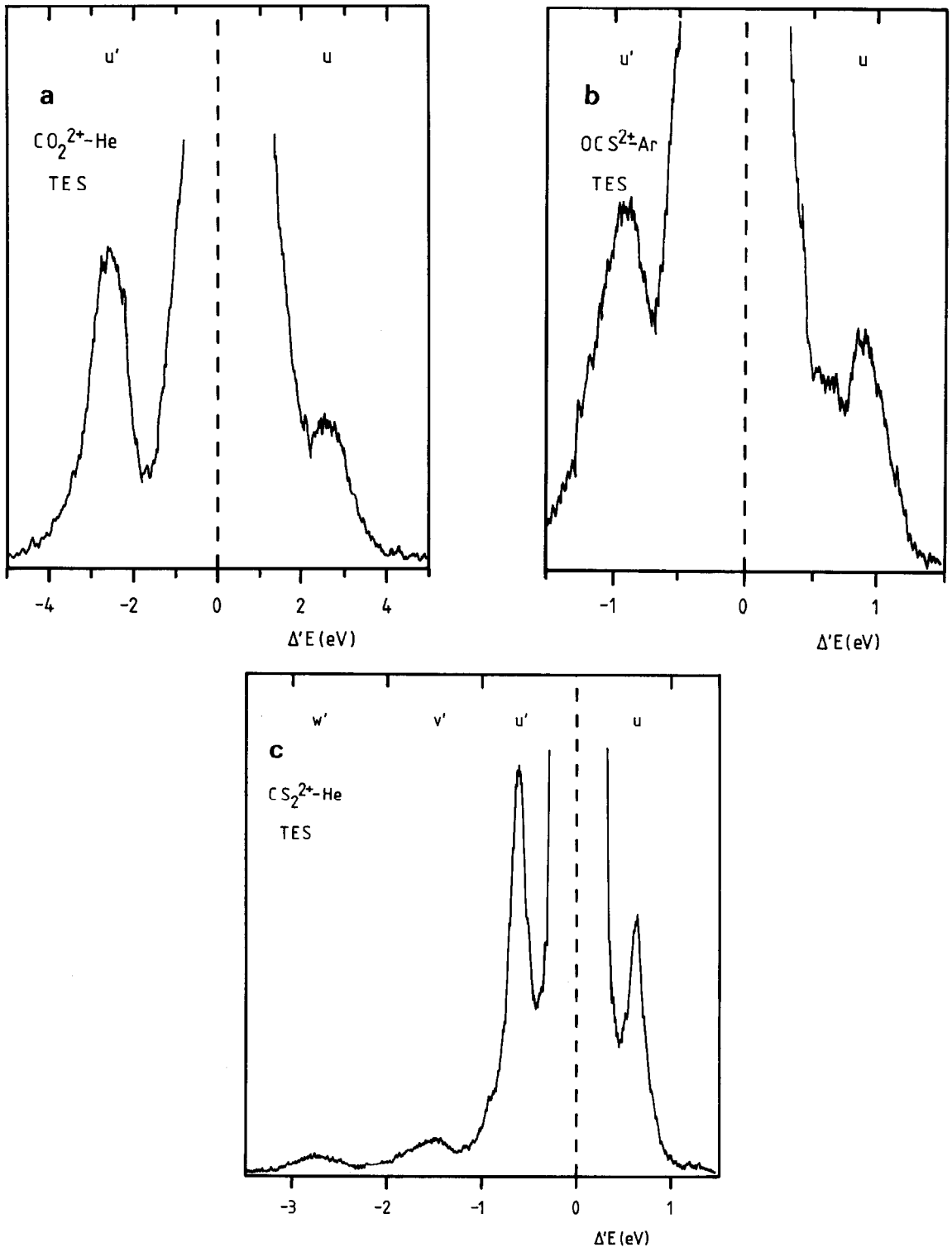

Fig. 4. Translational energy spectra of 6 keV TES collisions for (a) CO_2^{2+}, (b) OCS^{2+} and (c) CS_2^{2+} projectiles on He or Ar targets.

energy of ACB^{2+}. Since the rate of decrease of IV with decreasing E_e exceeds that of III, which exceeds that of II, we conclude that processes II, III (and IV) are due to excited ACB^{2+} states with successively increasing excitation energies.

3.2. TES

Translational energy spectra for the CO_2^{2+}–He, OCS^{2+}–He and CS_2^{2+}–He TES systems are shown in figs. 4a, 4b and 4c respectively. In each spectrum, peaks on the high-energy side of the main projectile beam (centred at $\Delta'E = 0$) represent superelastic collisions between an excited projectile ion and the He target, resulting in conversion of internal excitation energy into translational energy; at small scattering angles, the recoil velocity of the target is negligible, so that superelastic peaks reflect the excited-state populations in the incident ion beam. Low-energy peaks ($\Delta'E < 0$) are due to inelastic collision leading to internal excitation of either projectile or target. The choice of He as target effectively eliminates the latter possibility, since $E_v(\mathrm{He}(1s^2\,{}^1S) \rightarrow \mathrm{He}(1s2s\,{}^3S)) = 19.81$ eV [29] is well outside the energy range accessible in the present TES experiments.

Data extracted from these TES distributions are summarised in table 3. The most significant observation is that the cross section for TES processes u, u' in CS_2^{2+}–He are at least an order of magnitude higher than for all other processes detected; this feature may be highlighted by comparing the main projectile beam width, at the peak maxima for TES processes. For CO_2^{2+}–He in particular, a very wide projectile beam width of 2.7 eV signifies that the relative intensity of peaks u, u' is small. For OCS^{2+}–He, the proximity of u, u' to the main projectile beam, $O\text{–}u \approx 0.9$ eV, necessitates a comparatively narrow main beam of 1.1 eV width so that u, u' can be detected; the loss of sensitivity incurred is reflected in the poor signal-to-noise ratio for the spectrum (fig. 4b). In the case of CS_2^{2+}–He, however, transitions u, u' can be readily resolved with a projectile beam width of only 0.6 eV; the corresponding projectile beam widths for transitions v' and w' are considerably larger, nevertheless. Bearing in mind that TES is known to approximately obey the optical electric dipole selection rules (especially for systems, such as the present, with insignificant spin–orbit interactions), we conclude that transitions u, u' for CS_2^{2+}–He TES are spin allowed, whereas all other processes are either spin forbidden, or involve initial states with low populations in the ACB^{2+} projectile beam.

4. Discussion

The ground electronic states of the neutral linear molecules CO_2, OCS and CS_2 have $^1\Sigma^+$ symmetry. (The added inversion symmetry of CO_2 and CS_2 is understood.) The outermost orbital configurations for these triatomics are respectively $4\sigma_g^2 3\sigma_u^2 1\pi_u^4 1\pi_g^4$, $6\sigma^2 5\sigma^2 1\pi^4 2\pi^4$ and $6\sigma^2 5\sigma_u^2 2\pi_u^4 2_g^4$. Single ionisation occurs by ejection of an electron from the highest-energy π orbital. Similarly, double ionisation to the lowest ($^3\Sigma^-$, $^1\Delta$, $^1\Sigma^+$) dicationic states is facilitated by the removal of two electrons from this orbital; both these ionisation

Table 3
Summary of TES data

Collision system	Peak locations $\Delta'E$ (eV)				Approximate projectile beam width (eV) [a]
	$0\text{–}w'$	$0\text{–}v'$	$0\text{–}u'$	$0\text{–}u$	
CO_2^{2+}–He [b]	–	–	$-2.6(\pm0.1)$	$2.6(\pm0.1)$	2.7
OCS^{2+}–He	–	–	$-0.9(\pm0.15)$	$0.9(\pm0.15)$	1.1
CS_2^{2+}–He	$-2.7(\pm0.1)$	$-1.5(\pm0.1)$	$-0.6(\pm0.05)$ [c]	$0.6(\pm0.05)$ [c]	0.6

[a] Measured at the maximum height of the most intense TES peak.
[b] High-energy tail present on projectile beam peak.
[c] These peaks are at least an order of magnitude more intense than the other TES peaks reported here, indicative of spin-conserving transitions.

processes are highly localised [1] on the external O and S atoms. The outermost π orbital is essentially non-bonding, corresponding to overlap between the well-separated O and S atoms, so that ionisation as above is unlikely to significantly modify the interatomic bond lengths and strengths. Therefore, vertical transitions from the ground vibrational level of the ground-state neutrals will populate the ground, or low-lying ionic vibrational levels. Indeed, photoelectron spectroscopy has shown [33] that photoionisation of CO_2, CS_2 occurs predominantly (80%) into the ground vibrational level of CO_2^+, CS_2^+ ($\tilde{X}\,^2\Pi_g$) respectively; the largest vibrational excitation energy corresponding to symmetric stretching is ≈ 0.14 eV for CO_2^+ and only ≈ 0.07 eV for CS_2^+. These values are probably typical of OCS^+ and also the three dications. Consequently, even if significant vibrational excitation accompanies a given SEC or TES reaction, the excitation energies E_{vib} involved will be relatively small, especially for CS_2, the measured spectrum for CS_2^{2+}–Ar SEC (fig. 2c, table 2) exhibits sharp peaks, indicating small vibrational population of CS_2^{2+} and/or small degree of vibrational excitation of CS_2^+ after SEC. Significantly, peak IV of fig. 2c is far broader than peaks II and III in particular, implying that the corresponding capture channel from $CS_2^{2+}(\tilde{c}\,^1\Sigma_u^-)$ involves considerable vibrational excitation. This feature is not surprising, since $CS_2^{2+}(\tilde{c}\,^1\Sigma_u^-)$ has predominantly the $\pi_u^{-1}\pi_g^{-1}$ configuration [1] obtained by removal of a low-energy π_u electron, instead of the π_g^{-2} configuration for $CS_2^{2+}(\tilde{X}\,^3\Sigma_g^-, \tilde{a}\,^1\Delta_g, \tilde{b}\,^1\Sigma_u^+)$.

We conclude from the above that the difference in vibrational excitation energies between $ACB^{2+}(\tilde{X}, \tilde{a}, \tilde{b})$ and $ACB^+(\tilde{X})$ states participating in SEC is small, so that the evaluation of double-ionisation energies of ACB, and excitation energies for ACB^{2+}, by charge transfer (using (4)) is valid, provided that unambiguous interpretation of SEC spectra is possible. Variation of ionising electron energy E_e (figs. 2 and 3) confirms that SEC processes I (fig. 2, table 2) involve capture from ground-state ACB^{2+}, whereas peaks II, III (and IV) are due to SEC from successive excited projectile states (see section 3).

Using the average value of the existing appearance energy measurements (see table 1) for the triatomic dications ACB^{2+} in conjunction with spectroscopic data for the corresponding ACB^+ states (table 4) and the well-known first ionisation energies of the noble gases [34], then the approximate position of the ground state–ground state capture process:

$$ACB^{2+}(\tilde{X}) + R \rightarrow ACB(\tilde{X}) + R^+,$$

where

$$\begin{aligned} ACB = CO_2, &\quad \Delta E \approx 2.2 \text{ eV}; \\ = OCS, &\quad \approx 2.6 \text{ eV}; \\ = CS_2, &\quad = 1.8 \text{ eV}, \end{aligned} \tag{7}$$

can be estimated using (2). Comparing the approximate data in (7) with the measured exothermicities ΔE for the observed processes I in the SEC spectra (table 1) implies that peak I is indeed due to ground state–ground state capture. The only other feasible explanation for the spectra (fig. 2) would be that capture occurs, not to $ACB^+(\tilde{X})$, but to $ACB^+(\tilde{A})$. However, this latter interpretation would imply either that all previous measurements for $E_{el}(ACB^{2+})$ were in error by at least 2.6 eV, or alternatively that ACB^{2+} is formed exclusively in excited electronic states by electron impact, for each of CO_2^{2+}, OCS^{2+} and CS_2^{2+}! We exclude these possibilities. Therefore, the exact

Table 4
Spectroscopic data [a] for triatomic monocations

Ion	Designation	Appearance energy (eV)
CO_2^+	$\tilde{X}\,^2\Pi_g$	13.8
	$\tilde{A}\,^2\Pi_u$	17.3
	$\tilde{B}\,^2\Sigma_u^+$	18.1
	$\tilde{C}\,^2\Sigma_g^+$	19.4
OCS^+	$\tilde{X}\,^2\Pi$	11.2
	$\tilde{A}\,^2\Pi$	15.1
	$\tilde{B}\,^2\Sigma^+$	16.1
	$\tilde{C}\,^2\Sigma^+$	17.9
CS_2^+	$\tilde{X}\,^2\Pi_g$	10.1
	$\tilde{A}\,^2\Pi_u$	12.7
	$\tilde{B}\,^2\Sigma_u^+$	14.5
	$\tilde{C}\,^2\Sigma_g^+$	16.2

[a] Refs. [35,36].

exothermicities O–I (table 2) enable us to deduce the double-ionisation energies of ACB using (4), as discussed in section 1. Our charge-transfer values for $E_{el}(ACB^{2+}(\tilde{X}\,^3\Sigma_g^-))$, given in the final column of table 1, are in excellent agreement with previous data.

Spectroscopic assignments for the four lowest electronic states of CO_2^{2+}, OCS^{2+} and CS_2^{2+} were obtained by Millie et al. [1] by means of ab initio SCF CI calculations, assuming a fixed linear A–C–B^{2+} geometry, with bond lengths as in the neutral molecules. They conclude that the ground state of ACB^{2+} is in each case $^3\Sigma^-$, whereas the three subsequent electronic states are singlets ($^1\Delta$, $^1\Sigma^+$, $^1\Sigma^-$ respectively). The calculated excitation energies for these states are given in table 5, and show excellent agreement with proton double-charge transfer (DCT experiments performed by Fournier et al. [1,37,38]. The DCT process

$$\vec{H}^+ + ACB \rightarrow \vec{H}^- + ACB^{2+} \qquad (8)$$

strictly obeys the spin conservation rule, so that only singlet dication states are populated. Consequently, DCT data shown in tables 1 and 5 assume that the excitation energy of the lowest singlet state ($\tilde{a}\,^1\Delta$) of ACB^{2+} coincides with calculation in order to estimate the location of $ACB^{2+}(\tilde{X}\,^3\Sigma^-)$. The displacements I–II, I–III (and I–IV) in the present SEC spectra (fig. 2 and table 2) are in good accord with both DCT and calculation, as demonstrated by table 5. In particular, the resolution of the current apparatus permits precision that is comparable with, if not better than double-charge transfer; this is emphasised by the detection of $CO_2^{2+}(\tilde{b}\,^1\Sigma_g^+)$ (via process III of fig. 2a) not seen by DCT.

TES transitions for which spin angular momentum is conserved have high cross sections. The strong transitions (u, u') (at ± 0.6 eV, respectively) in CS_2^{2+}–He TES (fig. 4c, table 3) correspond to the II–III displacement (0.6 eV) for CS_2^{2+}–Ar SEC, suggesting that these transitions (u, u') are spin allowed $CS_2^{2+}(\tilde{a}\,^1\Delta_g) \rightleftharpoons CS_2^{2+}(\tilde{b}\,^1\Sigma_g^+)$. The CS_2^{2+}–Ar TES spectrum (fig. 4c) also exhibits weak processes (v', w') (at $\Delta'E = -1.5$ and -2.7 eV respectively) due to the spin-forbidden transitions $CS_2^{2+}(\tilde{X}\,^3\Sigma_g^-) \rightarrow CS_2^{2+}(\tilde{b}\,^1\Sigma_g^+, \tilde{c}\,^1\Sigma_u^-)$. The absence of clear evidence for $CS_2^{2+}(\tilde{X}\,^3\Sigma_g^-) \rightarrow CS_2^{2+}(\tilde{a}\,^1\Delta_g)$ is not surprising since this transition would appear (at $\Delta'E = -0.9$ eV) in a region of the TES spectrum dominated by u' and the low-energy tail of the main projectile beam.

Low cross sections for TES transitions in CO_2^{2+}–He TES are indicative, once more, of spin-forbidden processes. The observed transitions (u, u') at $\Delta'E = \pm 2.6$ eV are attributed to $CO_2^{2+}(\tilde{X}\,^3\Sigma_g^-) \rightleftharpoons CO_2^{2+}(\tilde{c}\,^1\Sigma_u^-)$. Failure to detect the spin-allowed transitions between singlet states is at first sight alarming in view of the fact that SEC predicts a significant population for $CO_2^{2+}(\tilde{a}\,^1\Delta_g, \tilde{b}\,^1\Sigma_g^+)$ in particular. Detection of the TES transitions $CO_2^{2+}(\tilde{a}\,^1\Delta_g) \rightleftharpoons CO_2^{2+}(\tilde{b}\,^1\Sigma_g^+)$ (with $\Delta'E = \mp 0.6$ eV respectively), for example, requires high energy resolution of < 0.6 eV; the presence of just one vibrational (symmetric stretch) level of

Table 5
Energy levels for triatomic dications

Ion	Designation [a]	DCT [b]	Calculation [c]	SEC [d]
CO_2^{2+}	$\tilde{X}\,^3\Sigma_g^-$	–	0	0
	$\tilde{a}\,^1\Delta_g$	1.2(±0.2) [e]	1.21	1.3(±0.2)
	$\tilde{b}\,^1\Sigma_g^+$	–	1.83	1.9(±0.3)
	$\tilde{c}\,^1\Sigma_u^-$	2.9(±0.3) [f]	2.87	2.7(±0.2)
OCS^{2+}	$\tilde{X}\,^3\Sigma^-$	–	0	0(±0.3) [g]
	$\tilde{a}\,^1\Delta$	1.1(±0.2) [e]	1.10	1.0 [g]
	$\tilde{b}\,^1\Sigma^+$	1.7(±0.2)	1.85	2.0(±0.1) [g]
	$\tilde{c}\,^1\Sigma^-$	3.8(±0.2)	4.06	–
CS_2^{2+}	$\tilde{X}\,^3\Sigma_g^-$	–	0	0
	$\tilde{a}\,^1\Delta_g$	0.9(±0.1) [e]	0.90	0.9(±0.1)
	$\tilde{b}\,^1\Sigma_g^+$	1.3(±0.2)	1.39	1.5(±0.1)
	$\tilde{c}\,^3\Sigma_u^-$	2.6(±0.3)	2.58	2.5(±0.2)

[a] Prehexes $\tilde{X}$, $\tilde{a}$, $\tilde{b}$... indicate possible states with increasing excitation energy, $\tilde{X}\,^3\Sigma^-$ being the ground dication state in each case.
[b] DCT accessed singlet dication states only [37,38].
[c] Full SCF CI PSI calculation [1].
[d] Present work.
[e] This level is taken to coincide with the corresponding calculated energy, since the ground triplet dicationic states are not accessed by DCT.
[f] Two interfering peaks at 2.5 and 3.2 eV are observed [1].
[g] $OCS^{2+}(\tilde{X}\,^3\Sigma^-)$ contributes a broad structure to the SEC spectrum. Measurement made with respect to $OCS^{2+}(\tilde{a}\,^1\Delta)$.

either participant singlet would broaden the observed peaks by > 0.14 eV [33], making the resolution of these transitions impossible using the present apparatus. Instead, such transitions would appear as broadening of the base of the main CO_2^{2+} projectile peak, centered at $\Delta'E = 0$; indeed, strong projectile beam tailing, especially for superelastic processes is possibly due to such transitions. In the case of OCS^{2+}–He TES (fig. 4b) resolution of processes (u, u') at $\Delta'E = \pm 1.0$ eV is possible only at the expense of sensitivity. Evidence for transitions at $\Delta'E \approx 0.7$ eV is also present. It is unclear whether to assign (u, u') to $OCS^{2+}(\tilde{X}\,^3\Sigma^-) \rightleftharpoons OCS_2^+(\tilde{a}\,^1\Delta_g)$ or the spin-allowed $OCS^{2+}(\tilde{a}\,^1\Delta_g) \rightleftharpoons OCS^{2+}(\tilde{b}\,^1\Sigma_g^+)$, or both, since the energies for these transitions are comparable; the latter process is promoted by spin-conservation considerations.

The excellent agreement between SEC and TES data obtained for the triatomic dications CO_2^{2+}, OCS^{2+} and CS_2^{2+} suggests future application of these techniques, in tandem, to elucidate the electronic levels of molecular dications which are inaccessible to standard spectroscopic analysis. Using the translational spectrometer, the following sequence of measurements is recommended:

(i) Appearance energy for the molecular dication (measured to ± 1 eV) using a standard Nier-type electron impact ion source.

(ii) High-resolution SEC experiments, using the appropiate choice of collision gas to ensure reasonable cross sections for ground (and near-ground) state–ground state capture (see section 1). Accurate translational energy scale calibration. Measurement of peak locations.

(iii) SEC data at a series of ionising electron energy settings, near the threshold for the molecular dications, facilitating the distinction of capture processes involving ground and excited projectile states.

(iv) High-resolution TES data, to confirm the assignment of energy levels (made possible by (ii) and (iii)) and to detect the presence of dication states with the same spin symmetry.

5. Conclusion

Using a novel high-resolution translational spectrometer, new experimental data for 6 keV single-electron capture by CO_2^{2+} and OCS^{2+} from selected rare gases and for translational energy spectroscopy of CO_2^{2+}, OCS^{2+} and Cs_2^{2+} on He are presented. For electron capture by CS_2^{2+} on Ar, the current result is superior to previous measurements [15].

The combined techniques of single-electron capture and translational energy spectroscopy applied to the triatomic dications CO_2^{2+}, OCS^{2+}, CS_2^{2+} provide values for the dicationic energy levels in excellent accord with previous theory and experiment. Provided that vibrational excitation can be shown to be insignificant the present research suggest future applications of these joint techniques to other multiply charged molecular ions, in order to measure their appearance and excitation energies.

Acknowledgement

We gratefully acknowledge support of this work by the Royal Society and University College of Swansea. GW thanks the British Council for financial support to visit Swansea, and PJ acknowledges the Science and Engineering research Council for the award of a research studentship.

References

[1] P. Millie, I. Nenner, P. Archirel, P. Lablanquie, P.G. Fournier and J.H.D. Eland, J. Chem. Phys. 84 (1986) 1259.

[2] W.E. Moddeman, T.A. Carlson, M.O. Krause, B.P. Pullen, W.E. Bull and G.K. Schweitzer, J. Chem. Phys. 55 (1971) 2317.

[3] F.H. Dorman and J.D. Morrison, J. Chem. Phys. 35 (1961) 575.

[4] A.S. Newton and A.F. Sciamanna, J. Chem. Phys. 40 (1964) 718.

[5] T.D. Märk and E. Hille, J. Chem. Phys. 69 (1978) 2492.

[6] R.G. Cooks, D.T. Terwilleger and J.H. Beynon, J. Chem. Phys. 61 (1974) 1208.

[7] B. Brehm, U. Frobe and H.P. Neitzke, Intern. J. Mass Spectrom. Ion Processes 57 (1984) 91.
[8] J.H. Agee, J.B. Wilcox, L.E. Abbey and T.F. Moran, Chem. Phys. 61 (1981) 171.
[9] J.A.R. Samson, P.C. Kemeny and G.N. Haddad, Chem. Phys. Letters 51 (1977) 75.
[10] P. Lablanquie, I. Nenner, P. Millie, P. Morin, J.H.D. Eland, M.J. Hubin-Franskin and J. Delwiche, J. Chem. Phys. 82 (1985) 2951.
[11] J.H. Beynon, A.G. Brenton and L.C.E. Taylor, Intern. J. Mass Spectrom. Ion Processes 64 (1985) 237.
[12] A.G. Brenton, M. Hamdan, P. Jonathan and J.H. Beynon, Intern. J. Mass Spectrom. Ion Processes, submitted for publication.
[13] E.Y. Kamber, P. Jonathan, A.G. Brenton and J.H. Beynon, J. Phys. B 20 (1987) 4129.
[14] D. Mathur, R.G. Kingson, F.M. Harris and J.H. Beynon, J. Phys. B 19 (1986) L575.
[15] D. Mathur, R.G. Kingston, F.M. Harris, A.G. Brenton and J.H. Beynon, J. Phys. B 20 (1987) 1811.
[16] Z. Herman, P. Jonathan, A.G. Brenton and J.H. Beynon, Chem. Phys. Letters 141 (1987) 433.
[17] Z. Herman, P. Jonathan, A.G. Brenton and J.H. Beynon, Chem. Phys., in preparation.
[18] J.O.K. Pederson and P. Hvelplund, J. Phys. B 20 (1987) L317.
[19] Q.C. Kessel, E. Pollack and W.W. Smith, in: Collision spectroscopy ed. R.G. Cooks (Plenum Press, New York, 1978).
[20] A.J. Illies and M.T. Bowers, Chem. Phys. 65 (1982) 281.
[21] J.H. Moore and J.P. Doering, J. Chem. Phys. 52 (1970) 1692.
[22] J.H. Moore, Phys. Rev. A 9 (1974) 2943.
[23] A. O'Keefe, A.J. Illies, J.R. Gilbert and M.T. Bowers, Chem. Phys. 82 (1983) 471.
[24] A. O'Keefe, R. Dérai and M.T. Bowers, Chem. Phys. 91 (1984) 161.
[25] N.J. Kirchner, A. O'Keefe, J.R. Gilbert and M.T. Bowers, Phys. Rev. Letters 52 (1984) 26.
[26] J.H. Moore, Phys. Rev. A 8 (1973) 2359.
[27] P. Jonathan and A.G. Brenton, Intern. J. Mass Spectrom. Ion Proc., submitted for publication.
[28] P. Jonathan, R.K. Boyd, A.G. Brenton and J.H. Beynon, Intern. J. Mass Spectrom. Ion Processes 68 (1986) 91.
[29] C.J. Porter, C.J. Proctor, T. Ast and J.H. Beynon, Croat. Chem. Acta 54 (1981) 407.
[30] J. Cuthbert, J. Farren and B.S. Prahallada Rao, J. Phys. B 1 (1968) 62.
[31] M. Lennon, R.W. McCullough and H.B. Gilbody, J. Phys. B 16 (1983) 2191.
[32] E.Y. Kamber, W.G. Hormis, A.G. Brenton, J.B. Hasted and J.H. Beynon, J. Phys. B 20 (1987) 105.
[33] J.H.D. Eland and C.J. Danby, Intern. J. Mass Spectrom. Ion Phys. 1 (1968) 111.
[34] C.E. Moore, Atomic energy levels, NBS Circular 467 (Natl. Bur. Std., Washington, 1949).
[35] H.M. Rosenstock, K. Draxl, B.W. Steiner and J.T. Herron, J. Phys. Chem. Ref. Data (1977), Suppl. 1.
[36] R.D. Levin and S.G. Lias, Ionization potential and appearance potential measurements 1971–1981, NSRDS–NBS71 (US Govt. Printing Office, Washington, 1982).
[37] J. Appell, J. Durup, F.C. Fehsenfeld and P.G. Fournier, J. Phys. B 6 (1973) 197.
[38] P.G. Fournier, J. Fournier, F. Salama, P.J. Richardson and J.H.D. Eland, J. Chem. Phys. 83 (1985) 241.